The destabilization paradox applied to friction-induced vibrations in an aircraft braking system

Fabrice Chevillot, Jean-Jacques Sinou, Guy-Bernard Mazet, Nicolas Hardouin, Louis Jezequel

The destabilization paradox applied to friction induced vibrations in an aircraft braking system

F. Chevillot[1,2], J-J. Sinou[1*], G-B. Mazet[2], N. Hardouin[2] and L. Jézéquel[1]

[1] Laboratoire de Tribologie et Dynamique des Systèmes UMR CNRS 5513
Ecole Centrale de Lyon, 36 avenue Guy de Collongue, 69134 Ecully Cedex, France

[2] Messier-Bugatti, Aircraft Braking Division
Zone Aéronautique Louis Bréguet, BP 40, 78140 Vélizy-Villacoublay, France

Abstract

Mechanisms of friction are known as an important source of vibrations in a large variety of engineering systems, where the emergence of oscillations is noisy and can cause severe damage to the system. The reduction or elimination of these vibrations is then an industrial issue that requires the attention of engineers and researchers together. Friction-induced vibrations have been the matter of several investigations, considering experimental, analytical and numerical approaches.

An aircraft braking system is a complex engineering system prone to friction-induced vibrations, and will be the matter of the work hereby presented. By considering experimental observations and by evaluating the mechanisms of friction involved, a complete non-linear model is built. The non-linear contact between the rotors and the stators is considered. The stability analysis is performed by determining the eigenvalues of the linearized system at the equilibrium point. Parametric studies are conducted in order to evaluate the effects of various system parameters on stability. A special attention will be given to the understanding of the role of damping and the associated destabilization paradox in mode-coupling instabilities.

Keywords: friction-induced vibration, mode-coupling instability, damping, stability analysis

1 Introduction

Friction-induced vibrations are a major concern in a broad variety of mechanical systems with rotating and sliding parts. The emergence of oscillations can be noisy and damageable for the integrity of the system and can cause accelerated wear of the components. It is especially the case in brakes, as well in automotive as in aeronautical or rail systems. Another common examples frequently encountered are the squeaking door, or the particularly unpleasant noise of a chalk applied on a blackboard.

The comprehension of the phenomena involved in these vibrations has been the matter of a number of investigations, and is still an active field of research in dynamics. It is assumed that vibrations induced by friction fall into four categories [1, 2, 3, 4]: stick-slip, variable dynamic friction coefficient, sprag-slip and

mode-coupling. Historically stick-slip is the first theory established to explain the emergence of vibrations. It is caused by a static friction coefficient higher than the dynamic friction coefficient. A mass sliding on a moving belt is a simple system that allows to reproduce this phenomenon. An expansion of this theory is given by a variable dynamic friction coefficient: a decrease in friction coefficient with relative sliding velocity is assumed to be a source of instability. This negative slope introduces a negative damping in the equations of motion that leads to single structural modes becoming unstable. However, friction-induced vibrations are not only the matter of tribological properties. Studies have shown that instability can occur with a constant coefficient of friction. The sprag-slip phenomenon, first proposed by [5] and then expanded by several investigators, is based on a geometrically-induced instability. Finally the fourth mechanism known to be a source of instability is the geometric coupling of the different degrees of freedom, that can occur given a constant coefficient of friction. In this case the instability is the result of the coupling of two structural modes of the system. This approach is largely used to reproduce friction-induced vibrations in mechanical systems.

In this study an aircraft braking system is considered. Based on experimental observations, a non-linear model for friction-induced vibrations is developed. It will be used for a better understanding of the role of damping on stability, and to evaluate to what extend damping can be introduced into the system to avoid any emergence of vibrations. The modelization of an aircraft braking system has been the matter of several papers before [6, 7, 8]. It has been also shown that stability can be affected by the design, and the effects of system parameters like hydraulic pressure and friction coefficient have been investigated. But most of the studies rely on undamped systems, or in the case of damped systems no full investigation of the effects of damping has been undertaken. And yet damping is commonly used in a wide variety of engineering systems: adding damping elements into one part of the system is assumed to reduce or eliminate friction-induced vibrations, but sometimes the results might be reversed. However, the role of damping on stability has been the subject of many papers. [9, 10, 11, 12, 13] have studied its effects on friction-induced vibrations of a two-degree-of-freedom system. They show that although damping in mode-coupling friction-induced vibrations is a complex phenomenon, some interesting results have been found. Thus, although dampers dissipate energy, increasing the damping does not lead systematically to the stabilization of the system if not introduced cautiously. That is why damping has to be examined in detail in order to avoid a bad design. This phenomenon, called the "'destabilization paradox"', was explained by Kirillov and Seyranian [14, 15]. Moreover, the role of the ratio of the damping parameters in the destabilization paradox is known from the study of different particular mechanical systems since at least 1930 (see [16, 17, 18, 19]).

The aim of this study is then to carry out an extensive analysis of the effects of damping on mode-coupling friction-induced instabilities on a fully non-linear model of an aircraft braking system. The non-linear contact between the rotors and the stators, and mechanisms between components are considered. The stability analysis is performed by determining the eigenvalues of the linearized equations of motion at the equilibrium point. Parametric studies with linear stability theory are conducted in order to determine the effects of system parameters including brake friction coefficient, non-linear stiffness and structural damping. In particular, the role of the damping ratio between two coupling modes will be examined, and it will be proved that the addition of damping can have in certain cases destabilizing effects. Finally, a design optimization by considering the Robust Damping Factor [9] will be used in order to avoid design errors.

2 System description and modelization

2.1 System description and dynamic tests

An aircraft braking system is given in Figure 1(a) where the main parts of the system are represented (except for the wheel and tyre). As shown the brake is composed of a stack of rotating brake discs (rotors) which engage the wheel, and stationary brake discs (stators) engaged by the torque tube. The torque tube is attached to the piston housing which is linked to the landing gear through a torque take-out rod. During the braking, the rotors and the stators are squeezed together by hydraulic pistons. Torque is produced by friction forces generated at the rubbing surface between the discs. The conversion of kinetic energy of the plane into heat in the brake discs causes the slowdown and the stopping of the aircraft.

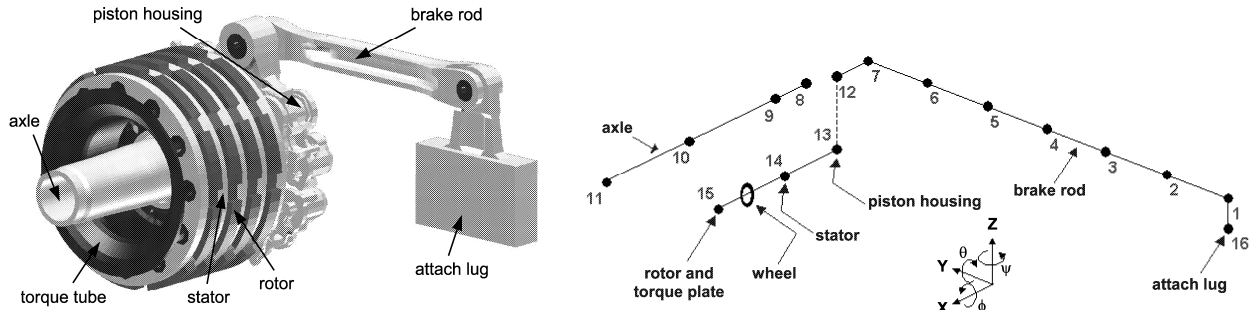

(a) Aircraft braking system (b) Parametric model of the brake

Figure 1: Aircraft braking system description

Dynamic tests using a fully instrumented aircraft brake are performed in order to analyze the vibratory behaviour of the brake. [8] present in detail the procedure of the test and give a view of the accelerometer locations on each part of the system. Different tests on several brake configurations allowed to identify in particular two important complex non-linear phenomena: squeal and whirl. Both appear at low frequency (in the 0-1000 Hz range) with amplitude oscillations potentially damageable for the integrity of the brake. On one hand squeal is defined as torsional vibrations of non-rotating brake parts around the axle. On the other hand whirl is defined as a motion of the end of the torque plate around the axle along with unphased pumping of the brake pistons.

2.2 Modelization and equations of motion

An analytical model has been developed in order to reproduce whirl and squeal instabilities. [6] presented the equations of motion and a model description simulating the squeal phenomenon. The model proposed is based on a geometric coupling between lateral translation and yaw of the rotors and stators. It predicts that instability can occur with a constant brake friction coefficient and without the use of brake negative damping. [8] presented a model for simulating the whirl phenomenon by using geometric coupling and sprag-slip approaches. Given these two works, a complete model for simulating both whirl and squeal instabilities will be built and used to study the dynamic behaviour of the brake.

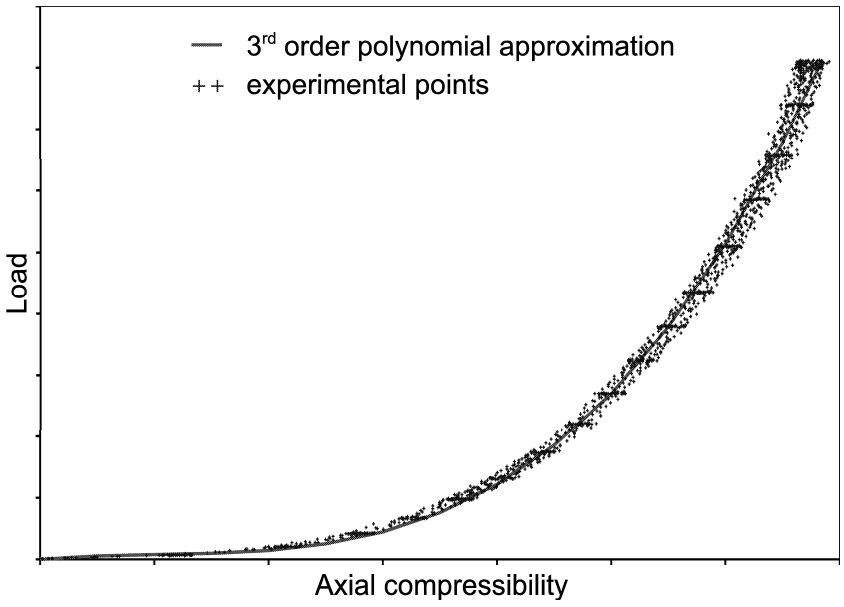

Figure 2: Non-linear approximation between load and axial compressibility of the discs stack

Experimental results have shown that the normal contact stress acting at the interface between the rotors and stators is highly non-linear. As shown in Figure 2, the load-deflection relationship can be expressed as a cubic polynomial with a good agreement with experimental results. The contact pressure is supposed uniformly distributed on the rubbing surface (a ring with inner radius Ri and outer radius Re as illustrated in Figure 3):

$$P(M) = \sum_{i=1}^{3} K_i \delta x^i \tag{1}$$

where M is a point of radial coordinate (r, θ), P is the load applied on the discs stack, δx is the relative displacement between the rotors and stators, and K_i (i=1 to 3) are the coefficients of the 3^{rd} order polynomial. The multi-stage brake is represented by a single rotor and stator with an effective brake friction coefficient of $\mu_{eq} = 2n\mu$ where n is the number of interfaces between the stators and rotors. It is assumed that the friction coefficient is uniform along the rubbing surface and that the rotor and stator friction surfaces are equivalent and always in contact. As given in the Coulomb friction model, the tangential stress is generated through this brake friction coefficient, in such a way that the normal and tangential elementary forces at the interface are expressed as:

$$N(r, \theta) = P(r, \theta) \tag{2}$$

$$T(r, \theta) = \mu_{eq} N(r, \theta) = \mu_{eq} P(r, \theta) \tag{3}$$

The normal relative compression δx is calculated by considering small displacements of the rotor and the stator:

$$x_{rotor}(r, \theta) = x_r + r sin\theta sin\theta_r - r cos\theta sin\psi_r \approx x_r + r\theta_r sin\theta - r\psi_r cos\theta \tag{4}$$

$$x_{stator}(r, \theta) = x_s + r sin\theta sin\theta_s - r cos\theta sin\psi_s \approx x_s + r\theta_s sin\theta - r\psi_s cos\theta \tag{5}$$

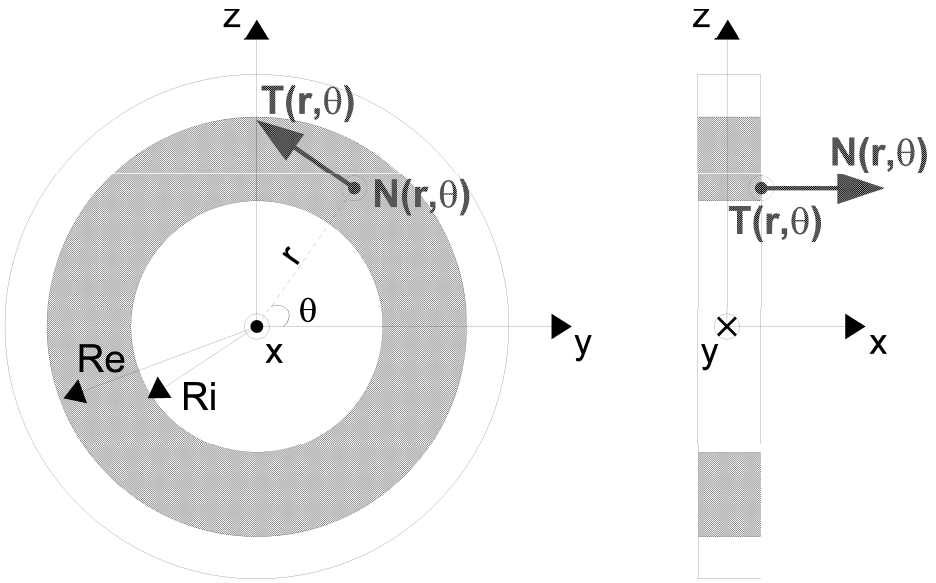

Figure 3: Friction modelization at the interface stator/rotor

that gives:

$$\delta x(r,\theta) = x_{stator}(r,\theta) - x_{rotor}(r,\theta) = (x_s - x_r) + rsin\theta(\theta_s - \theta_r) - rcos\theta(\psi_s - \psi_r) \tag{6}$$

where $x_s, x_r, \theta_s, \theta_r, \psi_s, \psi_r$ are respectively the stator and the rotor lateral displacements and rotations, as illustrated in Figure 1(b). Considering the cubic polynomial non-linear contact stress (1), the normal force F_X, the tangential forces F_Y, F_Z, the brake torque M_X and the yawing and pitching moments M_Y, M_Z due to friction can then be expressed by:

$$\begin{aligned} F_X &= \int_0^{2\pi}\int_{R_i}^{R_e} N(r,\theta) r dr d\theta = \int_0^{2\pi}\int_{R_i}^{R_e} \left(K_1\delta x(r,\theta) + K_2\delta x^2(r,\theta) + K_3\delta x^3(r,\theta)\right) r dr d\theta \\ &= K_1 A_2(x_s - x_r) + K_2\left(A_2(x_s - x_r)^2 + \frac{A_4}{4}(\theta_s - \theta_r)^2 + \frac{A_4}{4}(\psi_r - \psi_s)^2\right) \\ &\quad + K_3\left(A_2(x_s - x_r)^3 + \frac{3A_4}{4}(\theta_s - \theta_r)^2(x_s - x_r) + \frac{3A_4}{4}(\psi_s - \psi_r)^2(x_s - x_r)\right) \end{aligned} \tag{7}$$

$$\begin{aligned} F_Y &= -\int_0^{2\pi}\int_{R_i}^{R_e} T(r,\theta) sin\theta r dr d\theta = -\int_0^{2\pi}\int_{R_i}^{R_e} \mu_{eq} N(r,\theta) sin\theta r dr d\theta \\ &= -\mu_{eq}\left(K_1\frac{A_3}{3}(\theta_s - \theta_r) + K_2\frac{2A_3}{3}(\theta_s - \theta_r)(x_s - x_r)\right. \\ &\quad \left. + K_3\left(A_3(\theta_s - \theta_r)(x_s - x_r)^2 + \frac{3A_5}{20}(\theta_s - \theta_r)^3 + \frac{3A_5}{20}(\theta_s - \theta_r)(\psi_s - \psi_r)^2\right)\right) \end{aligned} \tag{8}$$

$$F_Z = \int_0^{2\pi}\int_{R_i}^{R_e} T(r,\theta) cos\theta r dr d\theta = \int_0^{2\pi}\int_{R_i}^{R_e} \mu_{eq} N(r,\theta) cos\theta r dr d\theta$$

$$= -\mu_{eq}\left(K_1\frac{A_3}{3}(\psi_s-\psi_r)+K_2\frac{2A_3}{3}(\psi_s-\psi_r)(x_s-x_r)\right.$$
$$\left.+K_3\left(A_3(\psi_s-\psi_r)(x_s-x_r)^2+\frac{3A_5}{20}(\psi_s-\psi_r)^3+\frac{3A_5}{20}(\psi_s-\psi_r)(\theta_s-\theta_r)^2\right)\right) \quad (9)$$

$$M_X = \int_0^{2\pi}\int_{R_i}^{R_e} T(r,\theta)r^2drd\theta = \int_0^{2\pi}\int_{R_i}^{R_e}\mu_{eq}N(r,\theta)r^2drd\theta$$
$$= \mu_{eq}\left(K_1\frac{2A_3}{3}(x_s-x_r)+K_2\left(\frac{2A_3}{3}(x_s-x_r)^2+\frac{A_5}{5}(\theta_s-\theta_r)^2+\frac{A_5}{5}(\psi_s-\psi_r)^2\right)\right.$$
$$\left.+K_3\left(\frac{2A_3}{3}(x_s-x_r)^3+\frac{3A_5}{5}(x_s-x_r)(\theta_s-\theta_r)^2+\frac{3A_5}{5}(x_s-x_r)(\psi_s-\psi_r)^2\right)\right) \quad (10)$$

$$M_Y = \int_0^{2\pi}\int_{R_i}^{R_e} N(r,\theta)sin\theta r^2drd\theta$$
$$= K_1\frac{A_4}{4}(\theta_s-\theta_r)+K_2\frac{A_4}{2}(\theta_s-\theta_r)(x_s-x_r)$$
$$+K_3\left(\frac{3A_4}{4}(\theta_s-\theta_r)(x_s-x_r)^2+\frac{3A_6}{24}(\theta_s-\theta_r)^3+\frac{3A_6}{24}(\theta_s-\theta_r)(\psi_s-\psi_r)^2\right) \quad (11)$$

$$M_Z = -\int_0^{2\pi}\int_{R_i}^{R_e} N(r,\theta)cos\theta r^2drd\theta$$
$$= K_1\frac{A_4}{4}(\psi_s-\psi_r)+K_2\frac{A_4}{2}(\psi_s-\psi_r)(x_s-x_r)$$
$$+K_3\left(\frac{3A_4}{4}(\psi_s-\psi_r)(x_s-x_r)^2\frac{3A_6}{24}(\psi_s-\psi_r)^3+\frac{3A_6}{24}(\psi_s-\psi_r)(\theta_s-\theta_r)^2\right) \quad (12)$$

with $A_k = \pi\left({R_e}^k - {R_i}^k\right)$ for k=2 to 6

The hydraulic pressure is then applied to the stator through the pistons, and the tire-ground drag force and the wheel bending load are introduced. The model built counts 16 nodes for a total of 70 degrees of freedom, as shown in Figure 1(b). The main addition compared with the studies presented by [8, 6] is the detailed modelization of the brake rod. By considering the interconnections between each element of the braking system, the global non-linear equations of motion take the form:

$$\mathbf{M}\ddot{\mathbf{x}} + \mathbf{C}\dot{\mathbf{x}} + \mathbf{K}\mathbf{x} = \mathbf{F}_{contact} + \mathbf{F}_{hydr} + \mathbf{F}_{drag} + \mathbf{F}_{load} \quad (13)$$

where $\ddot{\mathbf{x}}, \dot{\mathbf{x}}$ and $\mathbf{x}$ are respectively the 70-dimensional vectors of acceleration, velocity and displacement. $\mathbf{F}_{pressure}$ is the vector force due to brake hydraulic pressure, $\mathbf{F}_{contact}$ contains the linear and non-linear contact force terms at the stator and rotor interface, $\mathbf{F}_{drag}$ represents the tire-ground drag force, and $\mathbf{F}_{load}$ the bending load of the wheel. $\mathbf{M}, \mathbf{K}$ and $\mathbf{C}$ are the structural mass, global damping and stiffness matrices. The detailed expressions of the structural matrices are not given here, they are written by [8] in a case of a model without brake rod.

3 Stability analysis

To analyse the stability of the brake in a given configuration, the first step is to determine the steady-state operating point $\mathbf{x}_0$ for the full set of non-linear equations. It is given by solving the non-linear static equations of motion of the system:

$$\mathbf{K}\mathbf{x}_0 = \mathbf{F}_{contact}(\mathbf{x}_0) + \mathbf{F}_{drag}(\mathbf{x}_0) + \mathbf{F}_{hydr} + \mathbf{F}_{load} \tag{14}$$

Assuming that the tire-ground drag force is only dependent on the brake torque M_X, the previous equation can be written as:

$$\mathbf{K}\mathbf{x}_0 = \mathbf{F}_{NL}(\mathbf{x}_0) + \mathbf{F}_{hydr} + \mathbf{F}_{load} \tag{15}$$

where $\mathbf{F}_{NL}$ contains all the non-linear terms of $\mathbf{F}_{contact}$ and $\mathbf{F}_{drag}$.

Stability is then investigated for a small perturbation $\bar{\mathbf{x}}$ around the equilibrium point:

$$\mathbf{x} = \mathbf{x}_0 + \bar{\mathbf{x}} \tag{16}$$

so that the non-linear dynamic equations are:

$$\mathbf{M}\ddot{\bar{\mathbf{x}}} + \mathbf{C}\dot{\bar{\mathbf{x}}} + \mathbf{K}(\mathbf{x}_0 + \bar{\mathbf{x}}) = \mathbf{F}_{NL}(\mathbf{x}_0 + \bar{\mathbf{x}}) + \mathbf{F}_{hydr} + \mathbf{F}_{load} \tag{17}$$

Thanks to equation (14) it gives:

$$\mathbf{M}\ddot{\bar{\mathbf{x}}} + \mathbf{C}\dot{\bar{\mathbf{x}}} + \mathbf{K}\bar{\mathbf{x}} = \mathbf{F}_{NL}(\mathbf{x}_0 + \bar{\mathbf{x}}) - \mathbf{F}_{NL}(\mathbf{x}_0) \tag{18}$$

The next step is to linearize the non-linear terms contained by $\mathbf{F}_{NL}$ around the equilibrium point:

$$\mathbf{F}_{NL}(\mathbf{x}_0 + \bar{\mathbf{x}}) = \mathbf{F}_{NL}(\mathbf{x}_0) + \mathbf{F}_{NL}(\bar{\mathbf{x}}) \tag{19}$$

with

$$\mathbf{F}_{NL}(\bar{\mathbf{x}}) = \sum_i \left.\frac{\partial \mathbf{F}_{NL}(\bar{\mathbf{x}})}{\partial \bar{x}_i}\right|_{\mathbf{x}_0} \bar{x}_i = \mathbf{K}_L(\mathbf{x}_0)\bar{\mathbf{x}} \tag{20}$$

Finally the stability is analysed by considering the equation:

$$\mathbf{M}\ddot{\bar{\mathbf{x}}} + \mathbf{C}\dot{\bar{\mathbf{x}}} + (\mathbf{K} - \mathbf{K}_L(\mathbf{x}_0))\bar{\mathbf{x}} = \mathbf{0} \tag{21}$$

that gives the Jacobian matrix $\mathbf{J}$ expressed by:

$$\mathbf{J} = \begin{bmatrix} \mathbf{0} & \mathbf{I} \\ -\mathbf{M}^{-1}(\mathbf{K} - \mathbf{K}_L(\mathbf{x}_0)) & -\mathbf{M}^{-1}\mathbf{C} \end{bmatrix} \tag{22}$$

Local stability around the equilibrium point $\mathbf{x}_0$ is discussed by calculating the eigenvalues of the matrix $\mathbf{J}$. For λ a complex eigenvalue of the form $\lambda = a + \imath b$, the stability criterion is: if a is negative or zero, the system is stable and no vibration occurs, and if a is positive then the system is unstable. The imaginary part b represents the pulsation (or the frequency by considering a factor of 2π) of the vibration. A representation of the evolution of the pulsations and the real parts against the brake friction coefficient are given in Figures 4 and 5. The graphs below are normalized towards the pulsation of the first instability $\omega_{0,1}$ and towards the

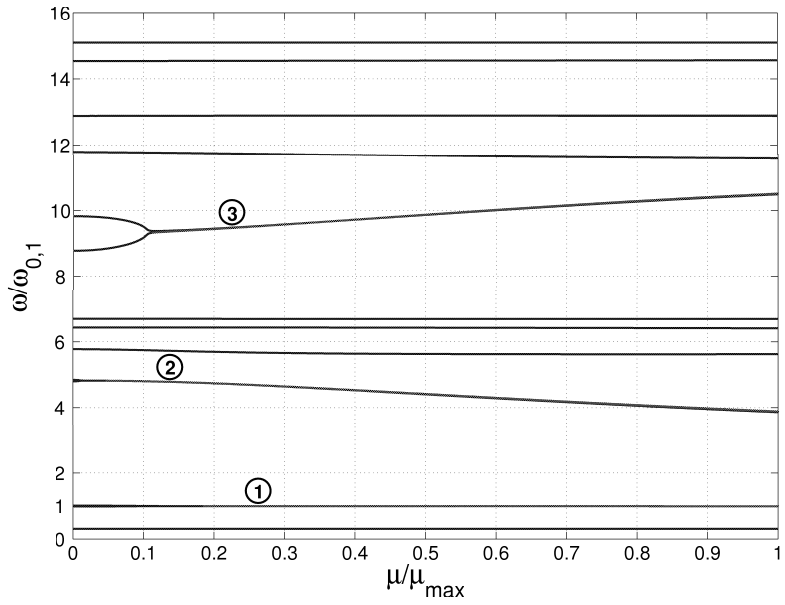

Figure 4: Evolution of the pulsations

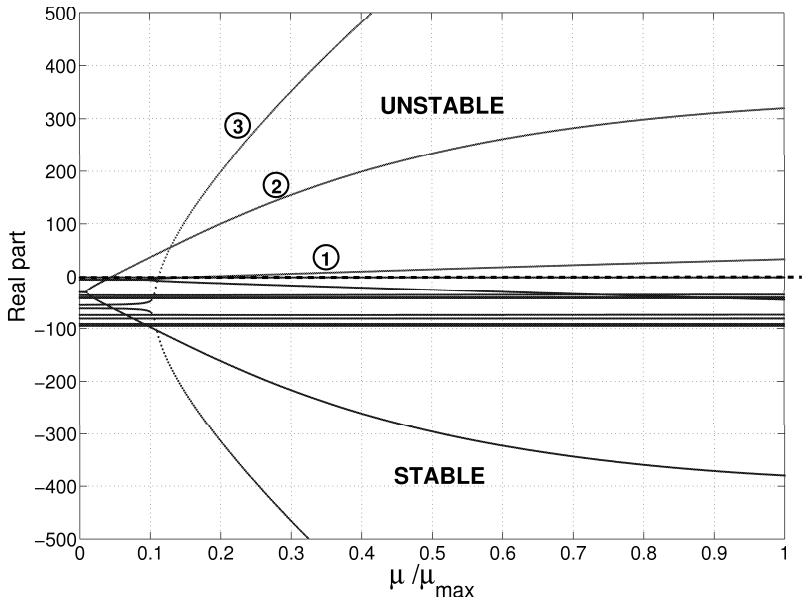

Figure 5: Evolution of the real parts

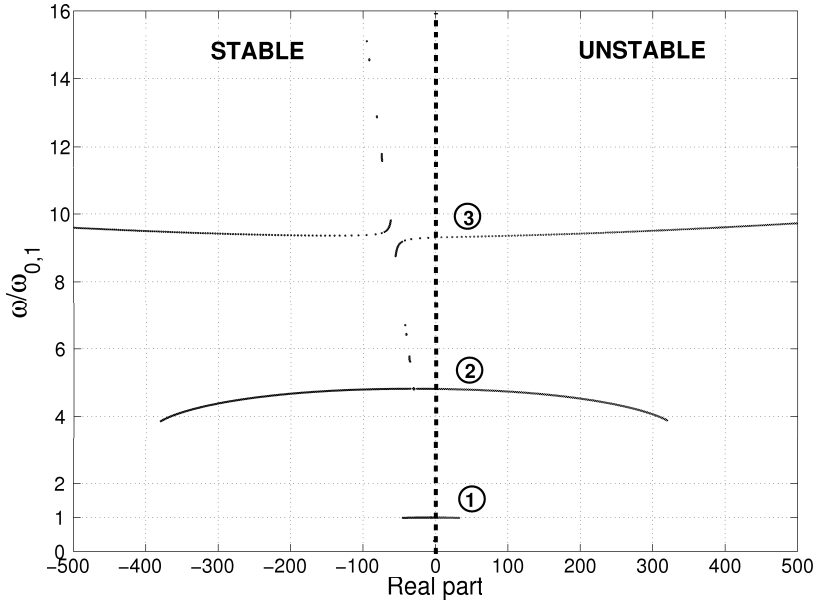

Figure 6: Evolution of the eigenvalues in the complex plane

maximum friction coefficient μ_{max} used in the study. It can be seen that in the frequency range of the study three coupling instabilities are calculated (in red on the figures). For low values of the friction coefficient the system is stable, and for higher values obviously the three instabilities can occur at the same time. At the present time, it is difficult to validate the scenario of several instabilities appearing together. It is rather thought that in practice one instability will be predominant and yield the major part of the oscillations. In the complex plane (Figure 6), the evolution of the pulsations against the real parts is represented. The stable and unstable zones are delimited by a real part equal to zero. For this first simulation, a standard modal damping has been introduced. Its effects can be observed in Figures 5 and 6: modal damping brings an offset in the real parts given by $\omega\eta$ (where ω is the pulsation of the mode and η the modal damping coefficient). Therefore, in that case the addition of damping pushes back the critical value of the friction coefficient for which the real part becomes positive and the instability appears. To identify the instabilities calculated, the analytical mode shapes are plotted for one period in Figures 7(a-c). The shaded mark defines the static position of the brake. An axial deflection of the axle and a complex rotating-bending motion of the rotor/stator producing a whirling motion of the torque plate and the piston housing is observed. Thus, the three instabilities match with the definition of the whirl given early. In particular, the second instability -known as the second whirl mode- has been recorded with high levels of acceleration during dynamics tests with a good agrement towards the frequency and the deformation. With a different brake configuration, a squeal coupling mode is calculated: its analytical deformation is given in Figure 7(d). So this model proves its ability to reproduce mode-coupling friction-induced vibrations as well whirl as squeal modes, with a constant brake friction coefficient and without the addition of negative damping. A good correlation with experimental tests is observed, which gives us confidence in the model.

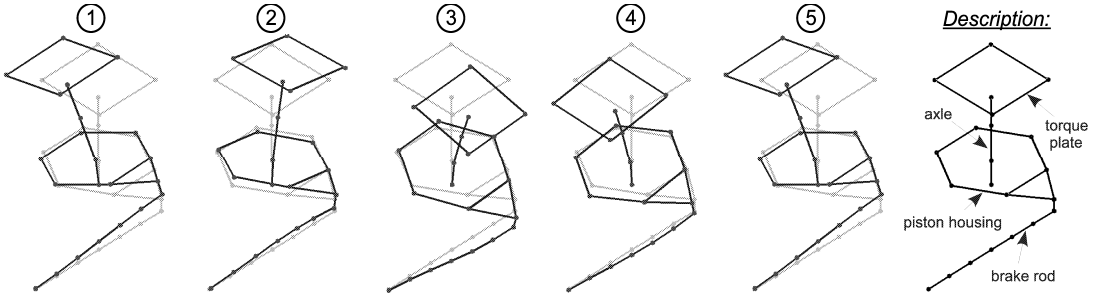

(a) Instability #1

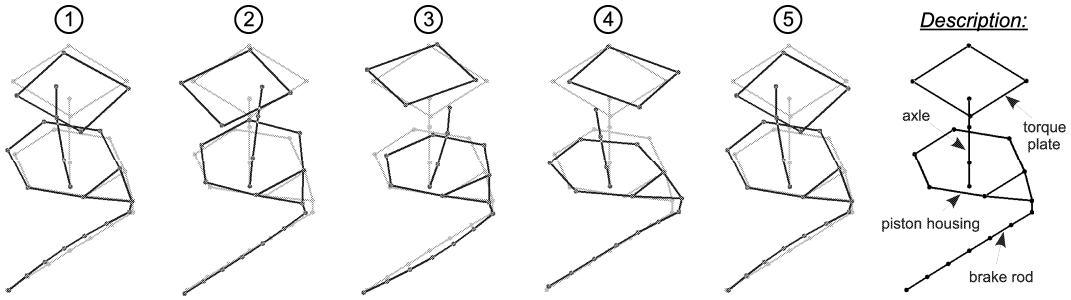

(b) Instability #2

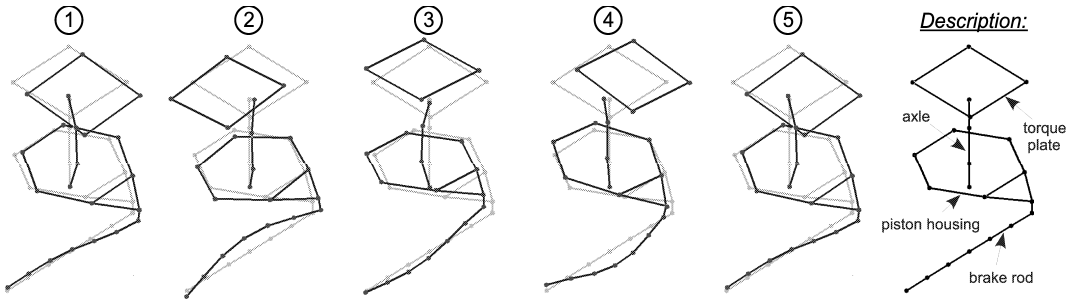

(c) Instability #3

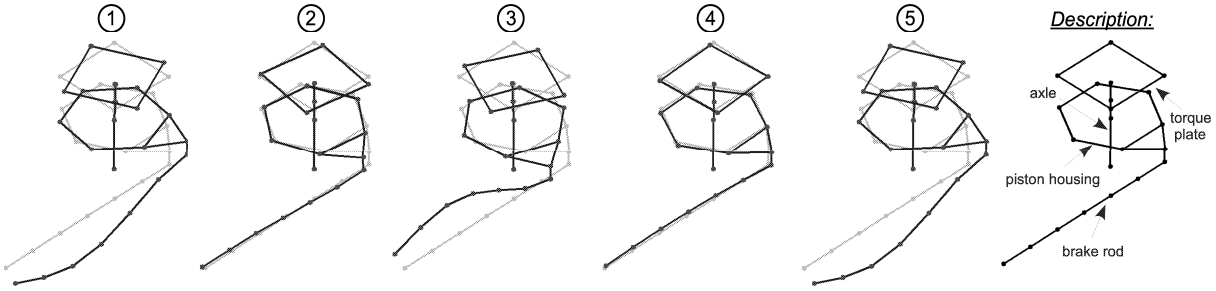

(d) Squeal instability

Figure 7: Analytical deformations of instabilities

4 The role of damping and the associated destabilization paradox

In order to avoid whirl and squeal instabilities and to evaluate the influence of various parameters, parametric studies have been made. They are conducted around a steady-state operating point with linear stability theory. A complete study of the effects of the damping ratio and an additional study on the non-linear stiffness of the discs stack compressibility are undertaken.

4.1 Effects of damping

In this part the effects of damping in mode-coupling instabilities are investigated. For each instability given in Figure 4, variations of the friction coefficient μ and of the modal damping coefficients η_1 and η_2 of the two coupling modes for each instability are considered. Damping is used in its modal approach, which means that we work in the modal base of the system. Thus, the damping of the 70 degrees of freedom yield a modal damping for each mode of the structure, depending on the elements dynamically involved in the deformation of the mode. Working in the modal base allows to reduce the number of parameters from 70 to only 2 for a lot easiest analysis. We will study the damping ratio η_1/η_2 as a key parameter: a constant modal damping amount is considered i.e. the sum $\eta_1 + \eta_2$ is taken constant. That means that we will study the effects of the distribution of damping between the two coupling modes. The effects of increasing proportional damping ($c_1 = \eta_1\omega_{0,1}$ and $c_2 = \eta_2\omega_{0,2}$ at the same time) have already been the matter of several investigations [11, 10]. Theirs conclusions were that adding proportional damping pushes back mode-coupling instabilities by increasing the stable region.

Figures 8(a) and 8(b) illustrate the change in the imaginary parts (the pulsations) and the real parts of the two eigenvalues giving instability #1. The white surface corresponds to the mode becoming unstable after the coupling, while the black surface illustrates the stable mode. there seems to be a value for the damping ratio η_1/η_2 for which the behaviour of the instability changes: below this specific value appearing near 1.0 the mode becoming unstable is the lowest pulsation one, and above this specific value the unstable mode is the highest pulsation one. For this specific value of η_1/η_2, the pulsations of the two modes are the same, and the difference between the real parts of the two eigenvalues is minimal. Figure 9 shows the variations in the stable and unstable regions. An optimal value of the damping ratio is observed: it corresponds to the specific ratio discussed above. At this damping ratio, the stable region is the greatest. For a very unproportional damping ratio (approaching zero), the system is more unstable that the undamped system.
As previously explained in [20, 21], the "'eigenvalue surfaces"' (i.e. the real and imaginary parts of eigenvalues as functions of the friction parameter and the ratio of two damping parameters) are self-intersected along the "'branch cut"', at the end of which there exists a double complex eigenvalue with the Jordan chain of length 2 with codimension 2 (i.e. the set of such eigenvalues in the plane of the two parameters is a point and in the space of three parameters it is a curve). In [21], it was shown that the point in the space of the three parameters corresponding to the double purely imaginary eigenvalue is a singularity of the boundary of the domain of asymptotic stability known as the "'Whitney umbrella"' [14, 15] (i.e. the domain of asymptotic stability is bounded by a nonsmooth surface having this singularity).

The same studies have been made for the two other mode-coupling instabilities calculated for this brake configuration. So in Figures 10-11 are given the graphs for instability #2, and in Figures 12-13 the graphes for instability #3. The same conclusions can be stated: that eliminates the effects of a particular behaviour of instability #2 in favour of a global behaviour of mode-coupling instabilities. It can then be

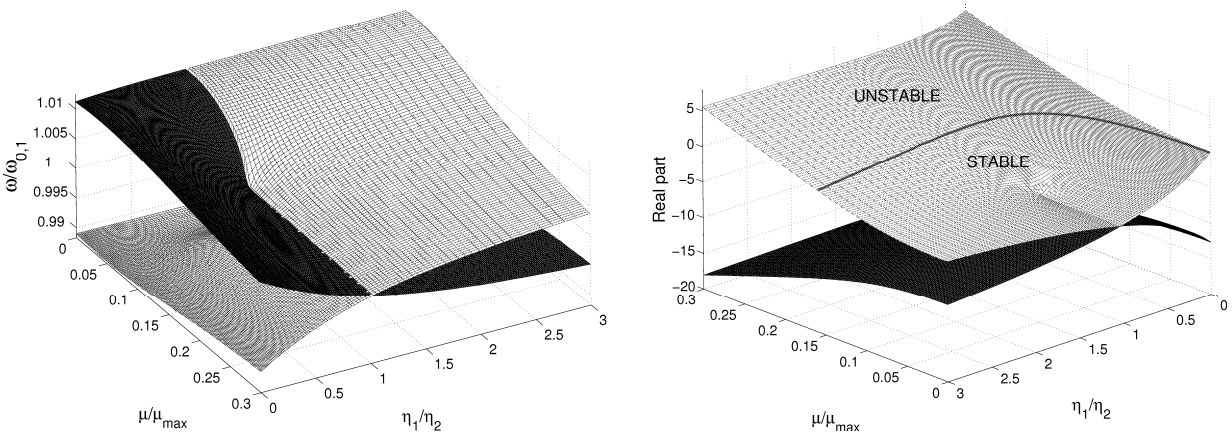

(a) Evolution of the pulsation of the two modes

(b) Evolution of the real part of the two eigenvalues

Figure 8: Stability versus μ/μ_{max} and η_1/η_2 for instability #1

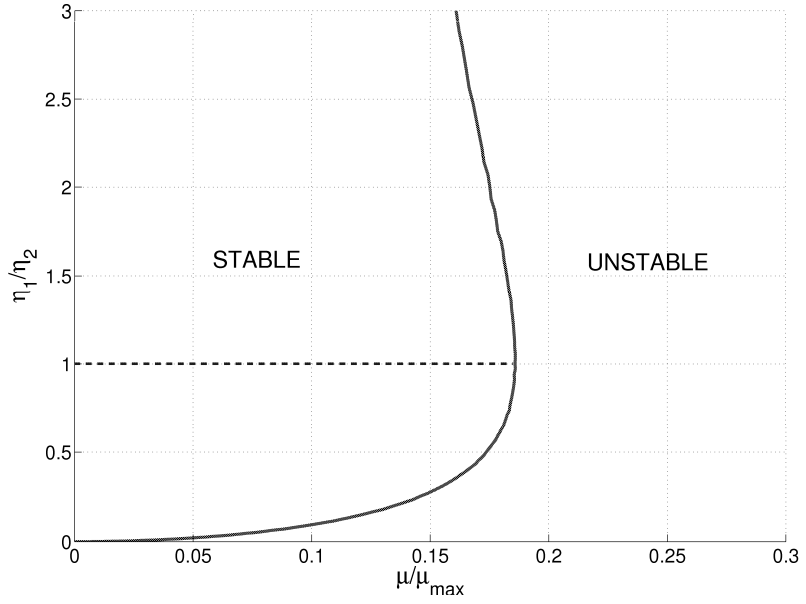

Figure 9: Stability (stable and unstable zones) versus μ/μ_{max} and η_1/η_2 for instability #1

concluded that in mode-coupling instabilities damping is useful to push back the unstable zone. An optimal damping ratio between the two coupling modes exists, and seems to be around a value of 1.0 (that means $\eta_1 \simeq \eta_2$). In the next chapter, thanks to a robust criterion, a more accurate study of the optimal value of the damping ratio will be undertaken. As it has been observed, damping has effects of the mode-coupling behaviour by changing the mode that becomes unstable when the instability occurs. However damping is not always beneficial: for low values of the damping ratio, the addition of damping leads to a decrease of the stable region to the extend that for very low values, the system is more unstable that the undamped system. So, the idea of adding damping in one part of the system to reduce or eliminate a vibration is not an advisable approach and can even lead to more damageable oscillations. This clearly illustrates the destabilizing effect of damping [14]: the system can be destabilized by adding damping elements which yet dissipate energy. From a practical point of view, the damping ratio can hardly reach zero because of the damping properties of the materials and the always dissipative contacts between the elements of the structure.

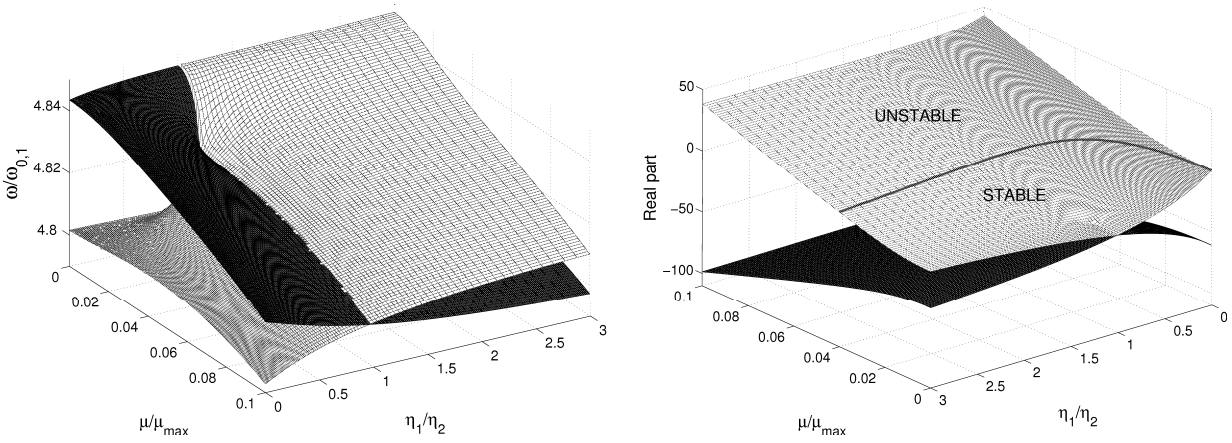

(a) Evolution of the pulsation of the two modes

(b) Evolution of the real part of the two eigenvalues

Figure 10: Stability versus μ/μ_{max} and η_1/η_2 for instability #2

4.2 Effects of the non-linear stiffness

A variation of the cubic coefficient of the 3^{rd} order polynomial approximating the non-linear relationship between load and relative displacement of the discs has been taken into account. It represents the dispersion resulting of several compressibility tests on a discs stack. The minimum, maximum and average curves are given in Figure 14. The study is made for the instability #2 (2^{nd} whirl) and for a friction coefficient $\mu/\mu_{max} = 0.045$. For a damping ratio of 1, this brake configuration is stable. In Figures 15(a) and 15(b) are given the evolution of the real parts and pulsations of the two modes versus the damping ratio η_1/η_2 and the cubic term K_3 of the non-linear stiffness around its average value $K_{3nominal}$. The white surface corresponds to the mode becoming unstable. First, the real part is not much affected by the non-linear stiffness. Then about the pulsations, the increase of the non-linear stiffness causes the decrease of the pulsation of the two

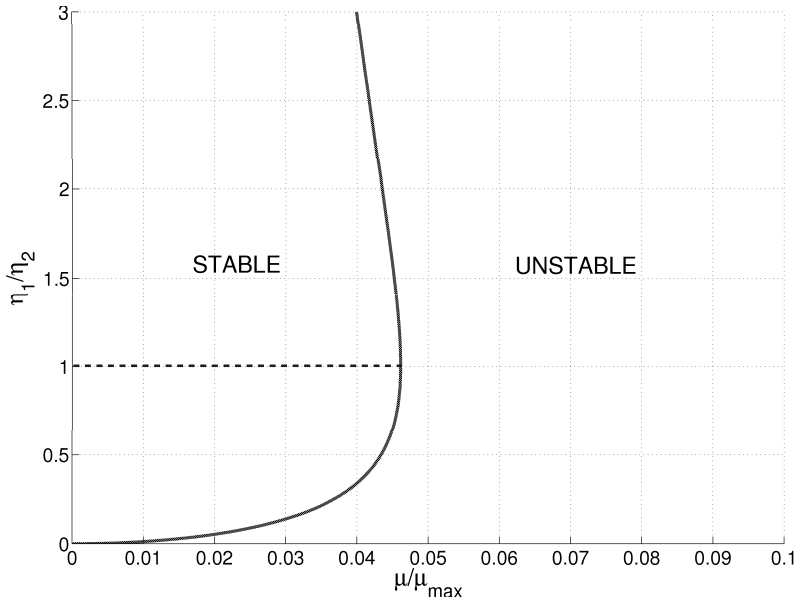

Figure 11: Stability (stable and unstable zones) versus μ/μ_{max} and η_1/η_2 for instability #2

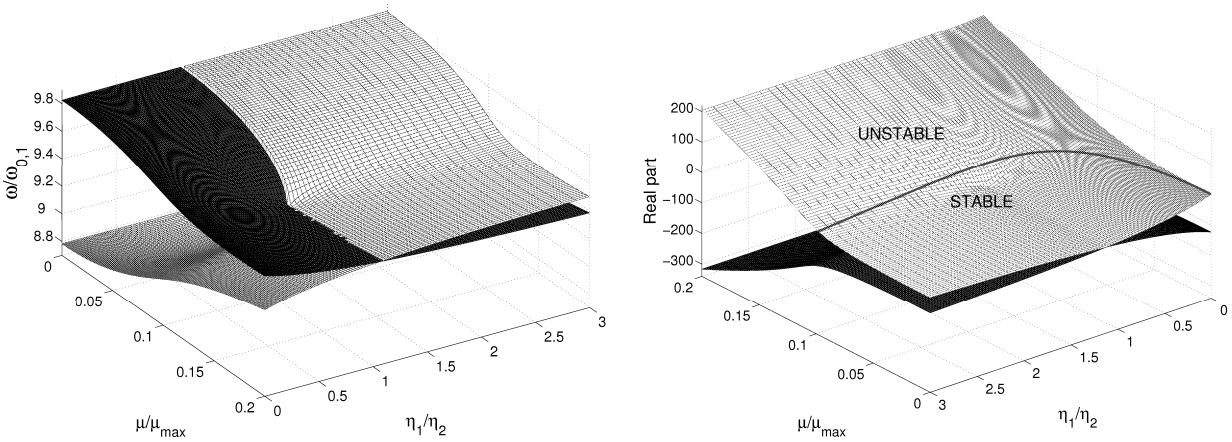

(a) Evolution of the pulsation of the two modes

(b) Evolution of the real part of the two eigenvalues

Figure 12: Stability versus μ/μ_{max} and η_1/η_2 for instability #3

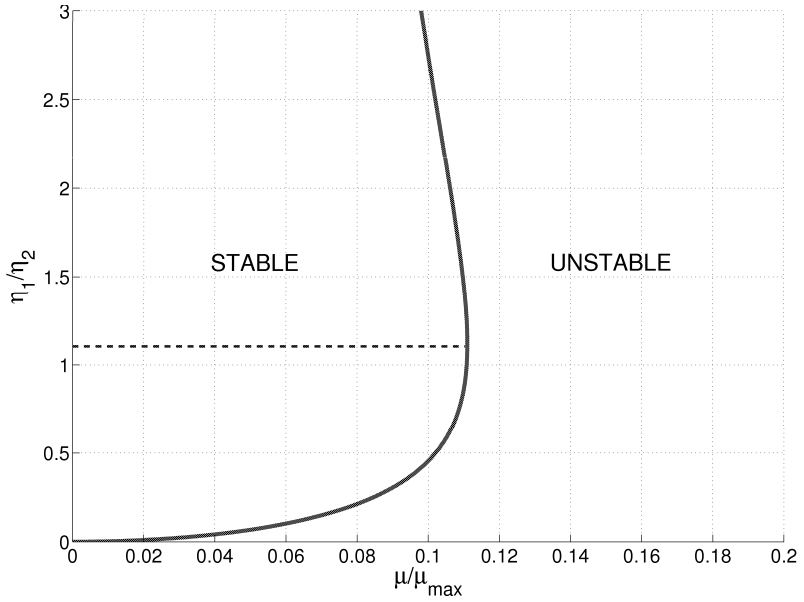

Figure 13: Stability (stable and unstable zones) versus μ/μ_{max} and η_1/η_2 for instability #3

modes. Concerning the damping ratio, the crossing in the pulsations for a specific value of the damping ratio is observed again. This behaviour is not dependent of the non-linear stiffness. For the optimum value of the damping ratio, the difference of the real parts is minimal. In Figure 16 giving the stable/unstable regions, it can be seen that the boundaries are not significantly affected by the variation of K_3 (that reflects the small effects on the real parts), even if a value of $K_3/K_{3nominal}$ around 0.9 seems to be an extremum for which the stable region is the smallest. Moreover a value of the damping ratio above 1.6 or under 0.6 leads to the destabilization of the system. Figure 17 illustrates the evolution of the compression of the discs stack versus the non-linear stiffness and the damping ratio. The three-dimensional graph is in practice a two-dimensional one, because the static position doesn't depend on the damping, as given in Equation 14. With an increase in the term K_3 the discs stack is stiffer. And for a given load, Figure 14 shows that a stiffer non-linear relationship results in a lower compressibility, which is thus illustrated by Figure 17.

5 Robust Damping Factor

To avoid design errors while using damping and to reduce mode-coupling instabilities in aircraft braking systems, a criterion was defined by [9]. Thus, the Robust Damping Factor (RD-Factor) was built to give the optimal damping ratio with regard to the stability of the system. Its definition is based on the observations made during the parametric studies presented in paragraph 4.1 which involve variations of the friction coefficient and the damping ratio at the same time. The best damping configuration is obtained when the critical value of the friction coefficient -for which the system becomes unstable- is the greatest. It as been observed that in that case the difference between the real parts $\Delta R = |Re(\lambda_{unstable}) - Re(\lambda_{stable})|$ is minimal. Moreover, the difference between the pulsations $\Delta F = |Im(\lambda_{unstable}) - Im(\lambda_{stable})|$ is minimal

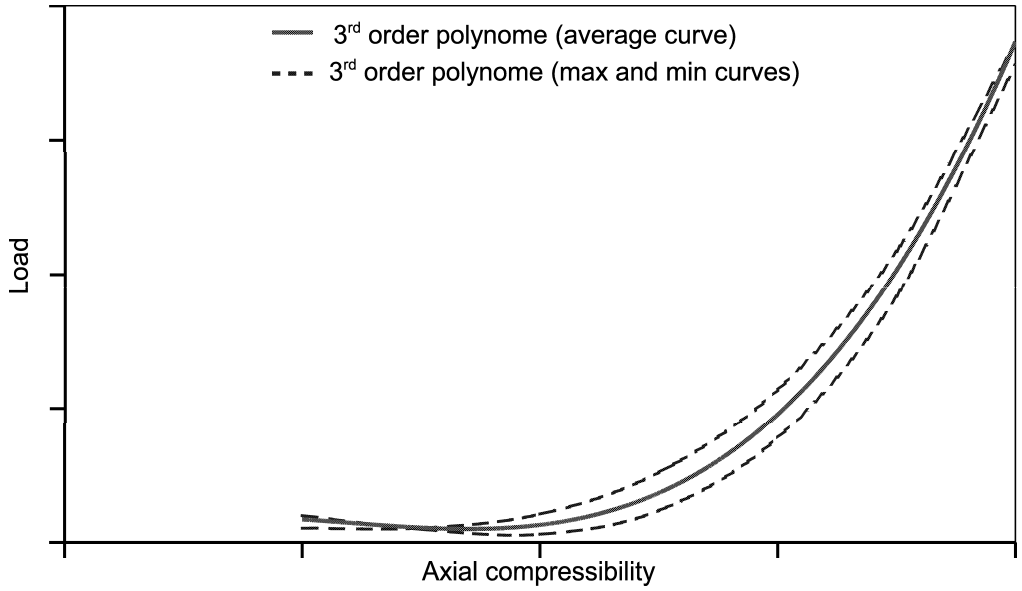

Figure 14: Non-linear compressibility of the discs stack with dispersion on the cubic term

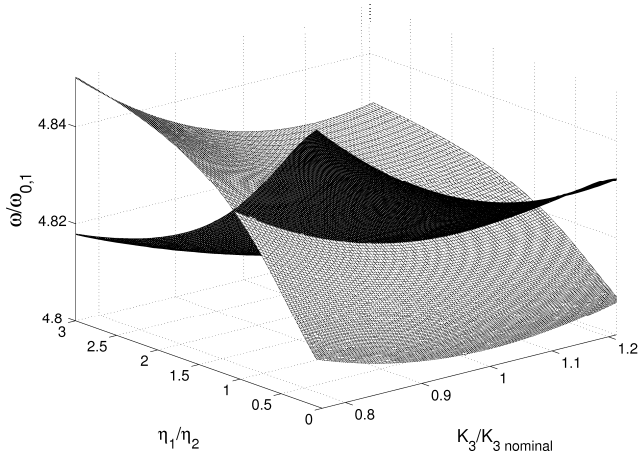

(a) Evolution of the pulsation of the two modes

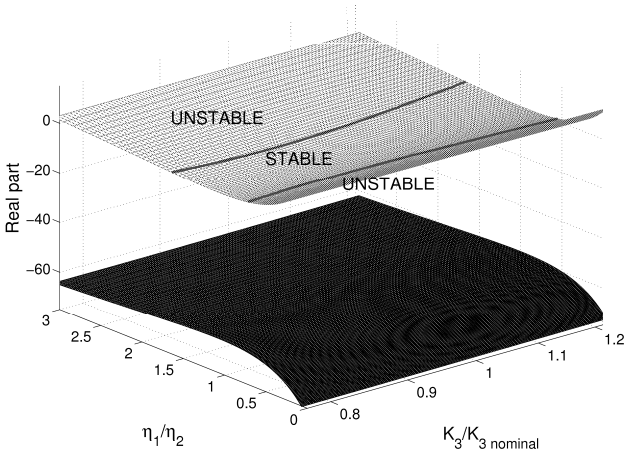

(b) Evolution of the real part of the two eigenvalues

Figure 15: Stability versus $K_3/K_{3nominal}$ and η_1/η_2 for instability #2

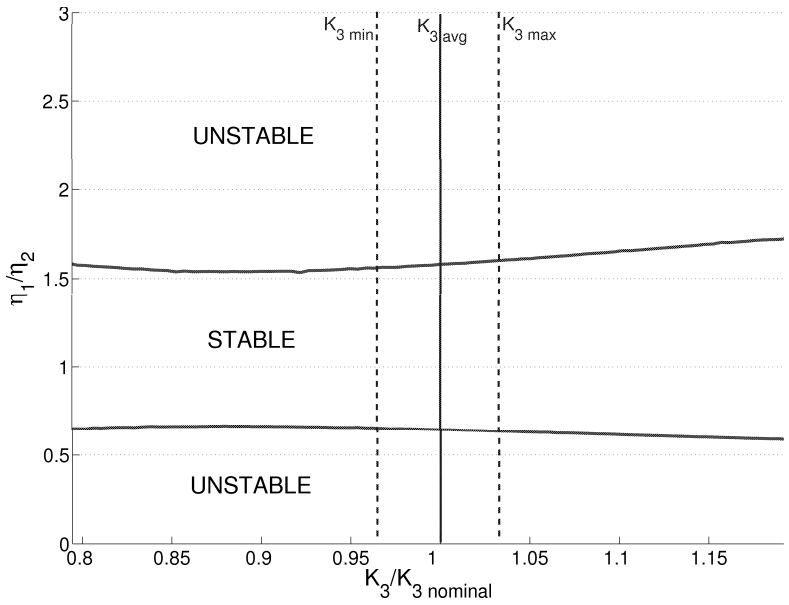

Figure 16: Stability (stable and unstable zones) versus $K_3/K_{3nominal}$ and η_1/η_2 for instability #2

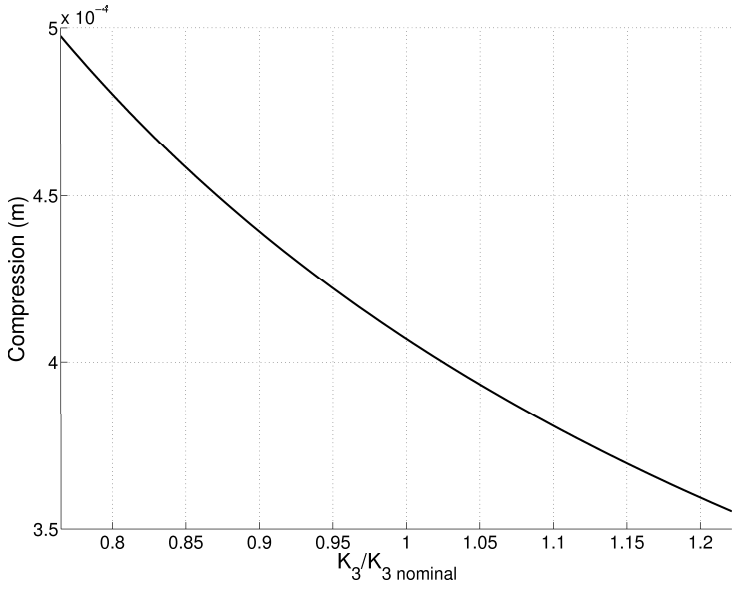

Figure 17: Evolution of the discs compression versus $K_3/K_{3nominal}$ for instability #2

when the merging of the two modes occurs. When increasing proportional damping, no variation in the difference of the real parts will be induced (the real parts will vary simultaneously), although the system is more stable. Thus, to take this third point into account, the value of $Max(Re(\lambda))$ is considered. Finally the RD-Factor is defined by:

$$\begin{array}{ll} RD-Factor = -Max(Re(\lambda)).log\left(\frac{\Delta F}{\Delta R+1}+1\right) & if \;\; Re(\lambda) \leq 0 \\ RD-Factor = 0 & if \;\; Re(\lambda) > 0 \end{array} \tag{23}$$

If the system is unstable (when $Re(\lambda) > 0$) the RD-Factor equals zero. The RD-Factor is defined in such a way that the greatest it is, the more stable the system is for the chosen parameters. The criterion is applied on each of the three whirl instabilities considered all along this study and on the squeal instability (Figures 18(a)-18(d)). On the maps of the RD-Factor, the most suitable damping ratio is well highlighted. It reflects the fact that for a given value of the friction coefficient, the introduction of unproportional damping is not optimal. For the squeal mode in Figure 18(d), it can be seen that the optimum damping ratio slightly increases with the friction coefficient, while it remains constant for the three whirl instabilities. This can be explained by the particular dynamic behaviour of the brake in this configuration: the squeal instability is perturbed by the proximity of the second whirl instability whose frequency is very close. To further our understanding of the most suitable damping ratio, a comparison with the pulsation ratio $\omega_{0,2}/\omega_{0,1}$ is given in Figure 19: there is a very good correlation between the optimum damping ratio and the frequency ratio. The conclusion of that is that in mode-coupling instabilities, the most suitable damping distribution corresponds to a proportional damping. That means the relation $\eta_1\omega_{0,1} = \eta_2\omega_{0,2}$ highlighted in several papers in a case of a two-degrees-of-freedom has to be verified. However, the result is valid as long as no third structural mode is involved or interfere in the coupling phenomenon, as it is the case for the squeal instability given as example but not fully examined in this study.

6 Summary and conclusions

A non-linear model for the analysis of mode-coupling instabilities induced by friction of an aircraft braking system has been presented. It has been developed by using experimental observations in order to reproduce whirl and squeal instabilities. The non-linear behaviour of the normal stress between the stator and rotor is considered. Parametric studies have been conducted to determine the effects of damping on stability.
It has also been shown that damping can be stabilizing as well as destabilizing. The damping ratio of the two modes leading to a mode-coupling instability appears to be a key factor. Thus, the addition of damping can lead to the destabilization of the mechanical system although damping elements paradoxically allow to dissipate energy. With the use of a Robust Damping Factor, it has been established that the most suitable distribution of damping has to verify the relation $\eta_1\omega_{0,1} = \eta_2\omega_{0,2}$. Given a mode-coupling instability for which $\omega_{0,1} \approx \omega_{0,2}$, the relation can be in first approximation expressed by $\eta_1 \approx \eta_2$. At this optimal ratio, damping will always and at best stabilize the system, no destabilization because of damping is possible. Although the damping ratio can hardly reach zero because of the damping properties of the materials, it can significantly differ from a value close to 1 when adding damping elements into only one part of the system. This last approach sometimes used to avoid the emergence of vibrations must clearly be avoided given the results of this study.

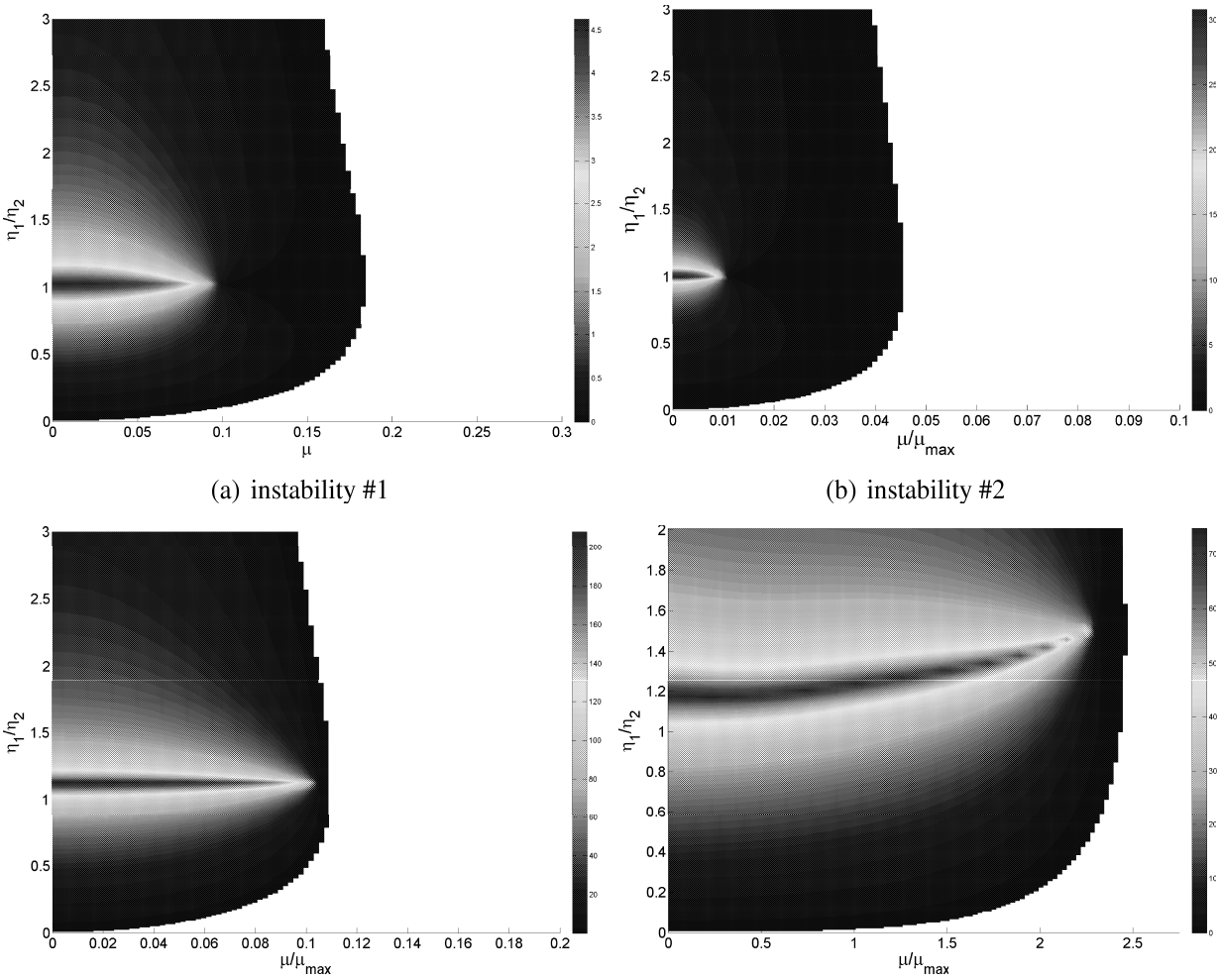

(a) instability #1

(b) instability #2

(c) instability #3

(d) squeal mode

Figure 18: Maps of the RD-Factor

instability	whirl #1	whirl #2	whirl #3	squeal
$\omega_{0,2}/\omega_{0,1}$	1.023	1.010	1.119	1.180
$(\eta_1/\eta_2)_{opt}$	1.03	1.00	1.125	1.175 (at $\mu = 0$)

Figure 19: Frequency ratio versus optimal damping ratio

References

[1] Kinkaid, N., O'Reilly, O., and Papadopoulos, P., 2003. "Automotive disc brake squeal". *Journal of Sound and Vibration,* **267**, p. 105–166.

[2] Ibrahim, R., 1994. "Friction-induced vibration, chatter, squeal, and chaos. part 1 : Mechanics of contact and friction". *ASME Design Engineering Technical Conferences,* **7**, pp. 209–226.

[3] Ibrahim, R., 1994. "Friction-induced vibration, chatter, squeal, and chaos. part 2 : Dynamics and modeling". *ASME Design Engineering Technical Conferences,* **7**, pp. 209–2269.

[4] Crolla, D., and Lang, A., 1991. "Brake noise and vibration - state of art". *Tribologie-Vehicle Tribology,* **18**, pp. p165–174.

[5] Spurr, R., 1961. "A theory of brake squeal". *Proc. Auto. Div. Instn. Mech. Engrs,* **1**, pp. 33–40.

[6] Liu, S., Özbek, M., and Gordon, J., 1996. "A nonlinear model for aircraft brake squeal analysis. part i: model description and solution methodology". *ASME Design Engineering Technical Conferences,* **3**, pp. 406–416.

[7] Liu, S., Özbek, M., and Gordon, J., 1996. "A nonlinear model for aircraft brake squeal analysis. part ii: stability analysis and parametric studies". *ASME Design Engineering Technical Conferences,* **3**, pp. 417–425.

[8] Sinou, J.-J., Dereure, O., Mazet, G.-B., Thouverez, F., and Jézéquel, L., 2006. "Friction induced vibration for an aircraft brake system. part 1: experimental approach and stability analysis.". *International Journal of Mechanical Sciences,* **48**, pp. 536–554.

[9] Sinou, J.-J., Fritz, G., and Jézéquel, L., 2007. "The role of damping and definition of the robust damping factor (rd-factor) for a self-exciting mechanism with constant friction". *Journal of Vibration and Acoustics,* **129(3)**, pp. 297–306.

[10] Sinou, J.-J., and Jézéquel, L., 2007. "Mode coupling instability in friction induced vibrations and its dependency on system parameters including damping". *Journal of European Mechanics - A/Solids,* **26**, p. 106–122.

[11] Hoffmann, N., and Gaul, L., 2003. "Effects of damping on mode-coupling instability in friction induced oscillations". *ZAMM · Z. Angew. Math. Mech.,* **83(8)**, pp. 524–534.

[12] Shin, K., Brennan, M., Oh, J.-E., and Harris, C., 2002. "Analysis of disc brake noise using a two-degree-of-freedom model". *Journal of Sound and Vibration,* **254**, pp. 837–848.

[13] Gallina, P., and Trevisani, A., 2003. "On the stabilizing and destabilizing effects of damping in wood cutting machines". *International Journal of Machine Tools and Manufacture,* **43**, p. 955–964.

[14] Kirollov, O., 2004. "Destabilization paradox". *Doklady Physics,* **49(4)**, pp. 239–245.

[15] Kirollov, O., and Seyranian, A., 2005. "The effetc of small internal and external damping on the stability of distributed non-conservative systems". *Journal of Applied Mathematics and Mechanics,* **69**, pp. 529–552.

[16] Bolotin, V., 1963. "Non-conservative problems of the theory of elastic stability". *Pergamon, Oxford*.

[17] Smith, D. M., 1933. "The motion of a rotor carried by a flexible shaft in flexible bearings". *Proceedings of the Royal Society of London. Series A, Containing Papers of a Mathematical and Physical Character,* **142(846)**, pp. 92–118.

[18] Crandall, S., 1995. "The effect of damping on the stability of gyroscopic pendulums". *Zeitschrift für angewandte Mathematik und Physik,* **46**, pp. 761–780.

[19] Kirillov, O., 2007. "Destabilization paradox due to breaking the hamiltonian and reversible symmetry". *International Journal of Non-Linear Mechanics,* **42(1)**, pp. 71–87.

[20] Seyranian, A., Kirillov, O., and Mailybaev, A., 2005. "Coupling of eigenvalues of complex matrices at diabolic and exceptional points". *Journal of Physics A: Mathematical and General,* **38(8)**, pp. 1723–1740.

[21] Arnold, V., 1983. "Geometrical methods in the theory of ordinary differential equations". *Springer, New York and Berlin*.